(*5*), we investigated whether *zig-4* is a possible interaction partner of the Robo/SAX-3 receptor, mutations in which cause VNC axon cross-over defects similar to those observed in *zig-4* mutants (*16*). We found, however, that unlike in *zig-4* mutant animals, the *sax-3* mutant phenotype is already manifested in freshly hatched L1 animals (*17*), and thus presumably represents an axon outgrowth defect rather than a maintenance defect. Consistent with such a notion, a *sax-3(0)zig-4(0)* double mutant shows additive defects in VNC disorganization (*17*). Taken together, *C. elegans* employs separate mechanisms for axon outgrowth and axon maintenance.

Several distinct models can be envisioned for how ZIG-4 and possibly other ZIG proteins mediate the maintenance function of PVT. ZIG-4 may "anchor" axons in the left and right VNC and thus prevent their flipping into the opposite fascicle by being an essential component of a ternary complex that ensures axon attachment to its environment in the left and right VNC. Because axon flip-overs in the absence of PVT-secreted ZIG cues require the presence of the contralateral analog of an axon, it could also be envisioned that an intrinsic attractive force of left/right analogous axons is directly antagonized by ZIG proteins, for example by ZIG proteins binding and inhibiting the activity of homophilic molecules presented by left/right contralaterally analogous axons. In a more indirect model, ZIG proteins could induce hypodermal cells to present specific stabilizing cues on the surface of the hypodermal ridge. Ultimately, the identification of the receptors for the ZIG proteins as well as their localization will illuminate the molecular mechanisms of ZIG protein action.

In summary, we have uncovered the existence as well as the cellular and molecular basis of a novel mechanism required to maintain correct axon positioning during specific stages of postembryonic growth and development. Axon fibers in any organism are subjected to various forms of mechanical stress and changing molecular and cellular environments during embryonic and postembryonic growth phases. The need to preserve the functional and structural integrity of the nervous system thus makes it likely that similar maintenance mechanisms, possibly also mediated by as yet uncharacterized 2-Ig domain proteins present in other metazoan genome sequences, are conserved across phylogeny.

References and Notes

1. R. M. Durbin, thesis, University of Cambridge, Cambridge, UK (1987).
2. In their electron microscopical reconstruction of the nervous system, White *et al.* had lost the tracking of the PVT axon in the posterior half of the animal (*18, 19*). Using several independent *gfp* reporters, we could show that the axon of PVT extends into the nerve ring. Another update to the White *et al.* report (*18*) is Durbin's finding that PVPR and not PVPL extends along the left side of the VNC (*1*).
3. W. G. Wadsworth, H. Bhatt, E. M. Hedgecock, *Neuron* **16**, 35 (1996).
4. X. C. Ren, S. Kim, E. Fox, E. M. Hedgecock, W. G. Wadsworth, *J. Neurobiol.* **39**, 107 (1999).
5. P. Sonderegger, Ed., *Ig Superfamily Molecules in the Nervous System* (Harwood Academic, Amsterdam, 1998).
6. Using standard sequence analysis tools, we identified the complete set of IgSF-only proteins in the *C. elegans* genome and examined their presumptive expression pattern using *gfp* reporter technology. The sequence and expression pattern analysis are shown in Web figs. 1 and 2, and Web table 1 (*20*).
7. Transgenic *gfp* reporter strains used to analyze VNC neuroanatomy are described in the Supplementary Methods (*20*).
8. See Web fig. 5 for electron micrographs of the hypodermal ridge of L1 animals (*20*).
9. An intrinsic homophilic affinity of bilateral analogs is suggested by the fact that the left and right axons of many bilaterally symmetric neurons, including AVKL/R, PVQL/R, PVPL/R, and HSNL/R, make direct contact with their contralateral analog in the nerve ring; moreover, axons of contralateral analogs that in wild-type animals both extend along the right VNC in tandem (e.g., AVBL/R, AVHL/R, AVAL/R, etc.) directly fasciculate with one another (*18*).
10. J. A. Lewis, C. H. Wu, H. Berg, J. H. Levine, *Genetics* **95**, 905 (1980).
11. O. Hobert, D. G. Moerman, K. A. Clark, M. C. Beckerle, G. Ruvkun, *J. Cell Biol.* **144**, 45 (1999).
12. B. Podbilewicz, J. G. White, *Dev. Biol.* **161**, 408 (1994).
13. J. E. Sulston, *Philos. Trans. R. Soc. London Ser. B* **275**, 287 (1976).
14. PVT cell fate and axon morphology were assessed using *unc-47Δ::gfp, zig-2::gfp*, and *zig-8::gfp*. *zig-4(0)* animals also appear indistinguishable from wild-type animals in regard to gross body morphology, locomotion, and the execution of simple behaviors.
15. D. M. Miller III, C. J. Niemeyer, *Development* **121**, 2877 (1995).
16. J. A. Zallen, S. A. Kirch, C. I. Bargmann, *Development* **126**, 3679 (1999).
17. Axon mispositioning defects were scored with the PVQL/R marker *oyIs14*. Newly hatched *sax-3(ky123)* L1s: 28.6% crossed-over, 25.7% laterally displaced ($n = 35$). Newly hatched *zig-4(gk34)* L1s: see Fig. 3D. In adults: *sax-3(ky123)*: 40.3% crossed-over ($n = 57$), *zig-4(gk34)*: 29% ($n = 114$), *sax-3(ky123)zig-4(gk34)*: 69.1% ($n = 55$).
18. J. G. White, E. Southgate, J. N. Thomson, S. Brenner, *Philos. Trans. R. Soc. London Ser. B* **314**, 1 (1986).
19. D. H. Hall, R. L. Russell, *J. Neurosci.* **11**, 1 (1991).
20. Supplementary material is available on *Science* Online at www.sciencemag.org/cgi/content/full/295/5555/686/DC1
21. For generation of constructs and transgenic animals see Supplementary Methods (*20*).
22. C. I. Bargmann, L. Avery, in Caenorhabditis elegans*: Modern Biological Analysis of an Organism*, H. F. Epstein, D. Shakes, Eds. (Academic Press, New York, 1995), vol. 48, pp. 225–250.

23. We are grateful to the Vancouver Knock-out consortium for providing the *gk34* allele, J. White and J. Hodgkin for supplying the raw EM data of several *C. elegans* strains from MRC/LMB files to the Center for *C. elegans* Anatomy, members of the worm community for providing transgenic *gfp* reporter strains, W. Raich for communicating results on *F02G3.1::gfp* expression, C. Bargmann for comments on bilaterality, T. Stephney for help with EM, J. Zhu and L. Diamond for expert technical assistance, the Hobert and Greenwald labs for support and discussion, and P. Sengupta, T. Jessell, R. Axel, I. Greenwald, and members of the Hobert lab for comments on the manuscript. Several strains were provided by the *C. elegans* Genetics Center, which is funded by the NIH. This work was funded by the Whitehall Foundation, the March of Dimes Foundation, an NIH postdoctoral fellowship to O.A. (5F32NS11107-02), and an NIH grant RR12596 to the Center for *C. elegans* Anatomy (D.H.H.). O.H. is a Searle and Irma T Hirschl Scholar, a Sloan Research Fellow, and a Klingenstein Fellow.

27 September 2001; accepted 7 December 2001

Dynamic Brain Sources of Visual Evoked Responses

S. Makeig,[1,3]* M. Westerfield,[1,3,4] T.-P. Jung,[1,3] S. Enghoff,[1] J. Townsend,[4] E. Courchesne,[4] T. J. Sejnowski[1,2,3,4,5]

It has been long debated whether averaged electrical responses recorded from the scalp result from stimulus-evoked brain events or stimulus-induced changes in ongoing brain dynamics. In a human visual selective attention task, we show that nontarget event-related potentials were mainly generated by partial stimulus-induced phase resetting of multiple electroencephalographic processes. Independent component analysis applied to the single-trial data identified at least eight classes of contributing components, including those producing central and lateral posterior alpha, left and right mu, and frontal midline theta rhythms. Scalp topographies of these components were consistent with their generation in compact cortical domains.

Increasing evidence suggests that correlated activity in neural populations is important for brain function and may be coupled to field potential oscillations over a wide range of frequencies (*1*). Most electroencephalographic (EEG) studies of human visual perception, however, have assumed the averaged event-related potential (ERP) evoked in humans by brief visual stimuli reflects neural activity within discrete, functionally defined visual cortical processing regions. In this view, response averaging removes background EEG activity (considered to be noise), whose time course is presumed to be independent of experimental events, as well as most artifacts produced by eye and muscle activity. Other researchers, by contrast, suggest that ERP features arise from alterations in the dynamics of ongoing neural synchrony generating the scalp EEG (*2–4*). By these

accounts, ERP features are produced through stimulus-induced resetting of the phase of ongoing field potential oscillations, a phenomenon observed in vitro (*5*).

Averaged ERPs evoked by sudden onsets of simple visual stimuli contain a prominent negative peak (N1) at 150 to 200 ms, modulated by attention (*6*), whose time course varies across scalp locations. The N1 is typically followed by a train of positive and negative deflections, termed "alpha ringing" from its resemblance to ongoing (8 to 12 Hz) alpha band EEG activity, whose time course also varies across scalp locations (*7*) consistent with observations that individual subjects may have multiple alpha rhythms with overlapping scalp topographies (*8, 9*).

To distinguish between the two hypotheses for the genesis of the average ERP, we compared the averaged ERPs and unaveraged EEG epochs time-locked to onsets of nontarget visual stimuli presented to the left visual field of 15 adult subjects in a spatial visual selective attention experiment [Web fig. 1 (*10*)] (*11, 12*). The frequency dependence and the scalp topography of the mean power in the single-subject average-ERP waveforms (Fig. 1A) resembled that of the unaveraged EEG (Fig. 1B). However, below 20 Hz the mean spectral amplitude of the poststimulus averaged ERP (Fig. 1A) was up to five times larger than that expected (Web fig. 3A) from the EEG spectrum of the single-trial responses (Fig. 1B), assuming that EEG phase (measured relative to stimulus onset) in the single trials averaged to form the ERP was randomly distributed (*13*). Further, at all scalp channels except the left occipital, the near 15 decibel (dB) increase in alpha power in the ERP waveforms beginning during the N1 interval (Fig. 1C) was not accompanied by any significant increase in alpha power in the single trials (Web fig. 3B) (*14, 15*).

Event-related intertrial coherence (ITC), a measure of the consistency across trials of EEG spectral phase at each frequency and latency window (*16*), revealed that during the N1 period, the uniform phase distribution across trials, existing before and during stimulus presentation, was replaced by a phase distribution weighted toward a dominant phase. This partial but significant "phase resetting" occurred following stimulus onsets in all scalp channels and EEG frequencies below 20 Hz (Fig. 1D). At 10 Hz in central posterior channels, ITC remained significant for 700 ms. Mathematically, the poststimulus ERP could be accounted for by the phase resetting of the EEG activity, as shown previously for auditory responses (*17*).

To test the implication of these results that the visual ERPs were not sums of a sequence of brief fixed-latency, fixed-polarity potential events, as often assumed, we sorted single-trial EEG epochs from each subject according to their poststimulus (0 to 293 ms) power at the peak alpha frequency (10.25 Hz) and separated the bottom and top 10% into two trial subsets. We then sorted trials in each subset according to their phase at the same frequency and time window. Plotting the phase-sorted single trials as color-coded horizontal lines in a rectangular image allowed visualization of the relationship between single-trial rhythmic EEG activity and its ERP average (Fig. 2, arrows). The ERP average of trials with strongest poststimulus alpha power (Fig. 2, upper panel) was large (>10 μV). Alpha phase of these trials was unevenly distributed from 200 ms before stimulus onset to 700 ms after stimulus onset. The prestimulus phase bias occurred because, consistent with previous reports by Brandt and others (*18–21*), poststimulus alpha activity in single trials tended to be largest in trials in which stimuli were presented at scalp-negative alpha phase.

For the subset of trials with weakest poststimulus alpha power (Fig. 2, lower panel), however, the ERP average was small (<1 μV), inconsistent with the assumption that the ERP sums fixed-latency, fixed-polarity potentials that are generated independent of the rest of the EEG. Figure 2 suggests that the fixed-latency, fixed-polarity components of early visual ERP records, if they exist at all, must be small (≪1 μV) (*2*).

If the N1 and other features of the visual ERPs arise primarily from phase resetting of ongoing EEG processes, which processes contribute to their generation? Because of their distance from the cortex, electrical potentials recorded at any scalp electrode sum the projected activities of multiple brain (and often nonbrain) sources. Under favorable circumstances, these can be separated by inde-

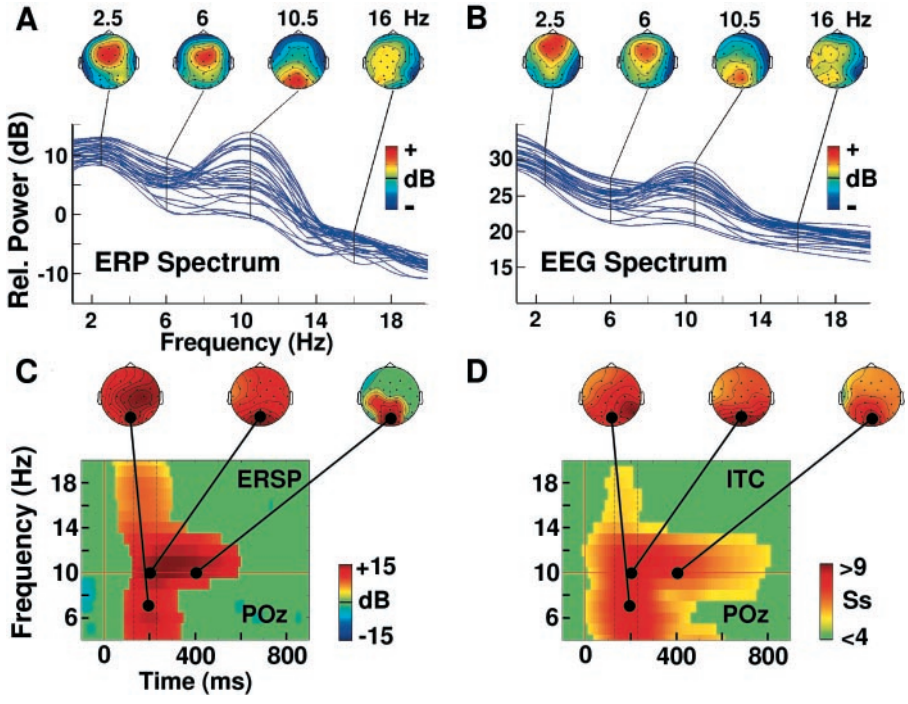

Fig. 1. Power spectra of unaveraged EEG and averaged ERP data have similar topographies. (**A**) Mean power spectra of 1-s ERPs averaging epochs time-locked to presentations of nontarget stimuli in the left visual field. Each trace represents one scalp channel (mean of 15 single-subject ERP spectra). Heads above, scalp distributions of power at four frequencies. (**B**) Mean power spectra, at each scalp channel, of the on-average 922 1-s EEG trial epochs averaged to create the single-subject ERPs. (**C**) Event-related spectral perturbation (ERSP) plot (*15*) showing mean poststimulus increases in spectral power of the single-subject ERPs, averaged across 15 subjects. Nongreen areas in the time/frequency plane that show significant ($P < 0.02$) poststimulus increases or decreases (see color scale) in log spectral power in the averaged ERP waveform at a central parietal electrode site (POz) relative to mean power in the averaged 1-s prestimulus ERP. Topographic scalp maps show topography of the poststimulus power increases in the ERP across all 29 scalp channels at three indicated points in the time/frequency plane. (Event-related increases and decreases in spectral power in the unaveraged single trials are shown in Web. fig. 3B). (**D**) Percentage of subjects with ($P < 0.02$) significant poststimulus intertrial coherence (ITC) (*16*), measuring the degree of phase resetting (i.e., phase consistency or phase locking) of EEG activity in single trials, at site POz.

[1]Computational Neurobiology Laboratory and [2]The Howard Hughes Medical Institute, The Salk Institute, 10010 North Torrey Pines Road, San Diego, CA 92037, USA. [3]Institute for Neural Computation; [4]Department of Neurosciences, School of Medicine; and [5]Department of Biology, University of California, San Diego, CA 92093, USA.

*To whom correspondence should be addressed. E-mail: smakeig@ucsd.edu

pendent component analysis (ICA) (*22–25*). Applied to EEG data, ICA finds spatial filters that separate the recorded activity into the sum of spatially fixed and distinct, temporally maximally independent component processes. To find sources of the ongoing EEG that contribute to the much smaller averaged ERP, we applied infomax ICA (*26*), separately for each subject, to concatenated 31-channel, 200-ms poststimulus EEG epochs (between 50 ms and 250 ms after stimulus onset) from ~3000 target and nontarget stimuli presented in the left, center, or right visual field (*27*).

ICA linearly decomposed each subject's EEG data in the N1 interval into 31 maximally independent components, each characterized by a different, fixed scalp map, showing the spatial projection of the component to each scalp channel, and a time course of activation in each trial. To determine which independent components were common across subjects, we performed cluster analysis on the component maps and activity spectra (*28*). Eight of the resulting clusters (Fig. 3) contained multiple components that were among the six largest contributors for each subject.

Components in the two lateral posterior clusters (labeled α_{LP} and α_{RP} in Fig. 3) accounted for the early lateral-occipital positivity (P1) as well as for part of the early part of the broad frontal N1 (Fig. 4, middle right). Their scalp maps generally resembled projections of single equivalent current dipoles in lateral occipital cortex (*29*). Concurrent, and more highly rhythmic, central-posterior alpha components (α_{CP}), found in nine subjects, made dominant contributions to alpha ringing without accompanying increases in alpha power (Fig. 4, left panel). In six subjects, the α_{CP} scalp map was best fitted by a source model comprising two synchronous dipoles located in left and right calcarine cortices. Two more component clusters (μ_{LC}, μ_{RC}) with centrolateral scalp maxima and ~10- and ~20-Hz spectral peaks (Fig. 4, right panel) accounted for separate left and right μ rhythms (*30–32*), and also contributed to the late N1. Scalp maps of these components were generally consistent with single compact cortical sources in the hand representation area of sensorimotor cortex. Another cluster of frontocentral components (FC) exhibited poststimulus intertrial phase coherence both in the theta and alpha bands that accounted for half the N1 variance at anterior channels (Fig. 4, center left). Single-dipole inverse source models of these components were concentrated in or near left dorsal anterior cingulate cortex (Web fig. 4). Together, the eight component clusters accounted for 77% of variance in the grand-mean ERP N1 as well as 79% of ERP variance in the subsequent alpha ringing period (Web fig. 5).

In the traditional model of ERP generation, averaging of sensory event-related EEG data is assumed to reveal a succession

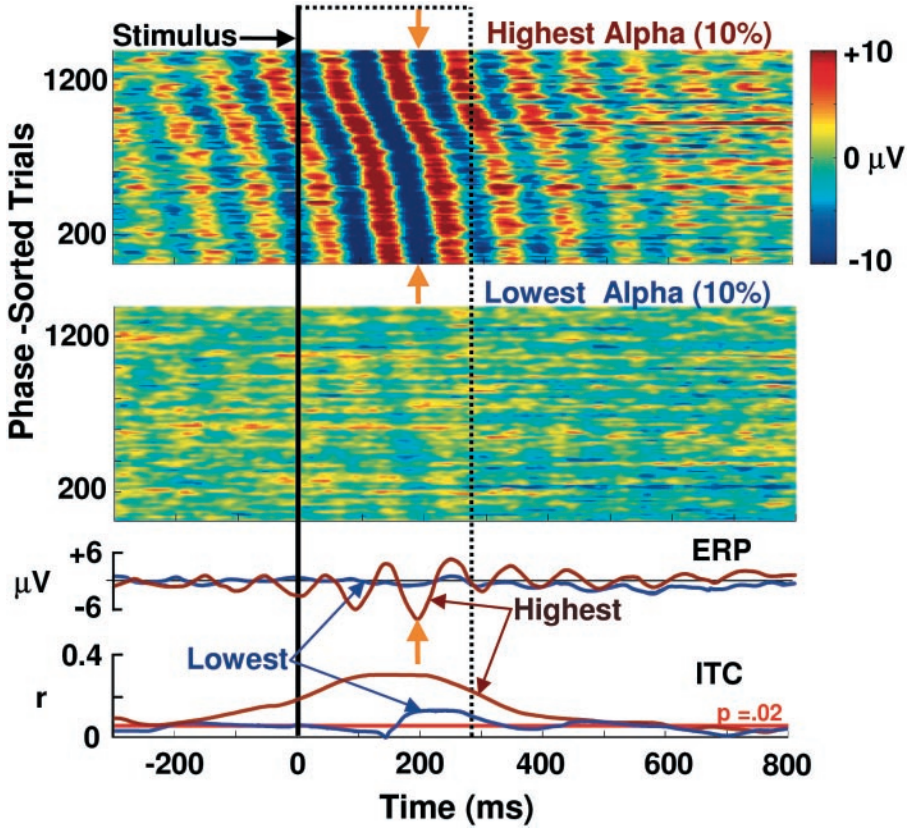

Fig. 2. The average ERP is produced by stimulus-induced phase resetting of ongoing EEG activity. Rectangular images, alpha phase-sorted "ERP-image" plots in which each horizontal line in the rectangular image represents a (color-coded) single trial, here at posterior central scalp site POz. Note the color μV scale on the right. The two ERP images show two (>1200) trial subsets consisting of the 10% of trials drawn from each of the 15 subjects having the highest or lowest power, respectively, at the peak alpha frequency (10.25 Hz) in the indicated poststimulus time window (0 to 293 ms, dotted lines). Before plotting, each trial subset was sorted (top-to-bottom) by its relative alpha phase in the same time window. The sigmoidal shape of the phase-sorted poststimulus alpha wave fronts (red and blue) in the highest-alpha trial subset (upper image) indicate the uneven distribution of poststimulus alpha phase. Upper traces below show the averaged ERPs for the high-alpha (brown trace) and low-alpha (blue trace) trial subsets. Lower traces show the time course of intertrial coherence (ITC) (*11*) at 10.25 Hz for the same trial subsets, together with (red line) the ($P = 0.02$) ITC significance level. The prominent negative (N1) peak in the highest-alpha ERP waveform (lower orange arrow) is the sum of more negative than positive single-trial values (between upper orange arrows) at the same response latency.

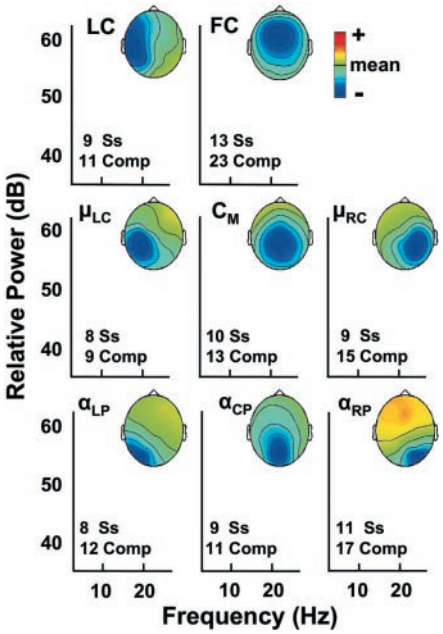

Fig. 3. Eight clusters of independent components of the poststimulus single-trial EEG data, derived by infomax ICA (*15*), accounted for most of the grand mean ERP. Each cluster contained components among the top six contributors to the N1 interval in the single-subject ERP and is represented by a mean scalp map and normalized power spectrum (mean $\pm$ 1 SD). Each cluster comprised 9 to 23 independent components from 8 to 13 of the subjects. Together, the eight clusters comprised 110 independent EEG components drawn from all 15 subjects. Unselected components had unique scalp maps or spectra, or represented nonbrain artifacts.

of reliably evoked ERP components (often identified with single response peaks) produced in sensory processing areas with fixed latencies and polarities, and to eliminate the (background) oscillatory EEG processes that are assumed to be unaffected by stimulation and irrelevant to brain stimulus processing. Our results extend previous conclusions (*2–4*) that many ERP features are instead produced by partial EEG phase resetting by suggesting a parsimonious explanation for the observed spatiotemporal complexity of both the N1 and the subsequent alpha ringing in these data as arising from stimulus-induced phase resetting of ongoing activity within multiple, maximally independent EEG domains. Although we do not suggest all features of averaged ERPs are necessarily generated by partial phase resetting of EEG processes without concurrent energy increases, for these data, phase resetting explains (i) why the ERP average of epochs with low single-trial alpha energy is so small (Fig. 2), (ii) why the strong, ~10-Hz ("alpha-ringing") peak in the power spectrum of the ERP (Fig. 1C) need not be accompanied by an event-related increase in alpha band EEG power in single trials, and (iii) why the latencies of the resulting ERP peaks need not match the (50 to 100 ms) latency of initial neural activation in visual areas.

That the scalp topographies of the EEG processes separated by ICA can be mostly fit by single equivalent current dipoles is consistent with their generation in compact cortical domains. These results suggest that the scalp EEG is largely the sum of a limited number of such processes, and that the location, orientation, and spectral character of these domains may be similar across subjects. Separation of EEG data by ICA into independent domains appears to reveal a new system different from the hierarchical organization of cortical areas involved in the representation of sensory information, a system involving synchronous electromagnetic field activity within relatively large independent EEG domains. Some physiological results suggest that the EEG domains that are partially phase reset to produce the ERP components (Fig. 3) may extend into more than one visual processing area (*33*). Neuromodulatory processes may be involved in regulating synchrony in large thalamocortical populations (*34*), whereas synchrony in small cortical domains is supported by networks of local inhibitory interneurons (*1, 35*). It is possible that the spatial extent of the EEG domains identified by ICA may be identified by concurrent EEG and functional magnetic resonance imaging (fMRI) (*36, 37*).

After a visual event, spatially distinct and otherwise independent EEG domains may also exhibit transient frequency-domain coherence that may not depend on stimulus-induced phase resetting. For example, during the N1 interval following presentation of face-image stimuli, local field potential signals recorded directly in fusiform gyrus and in several other human brain areas exhibit transient coherence in the alpha band (*38, 39*). This transient coherence may organize top-down brain responses and focus further processing of stimuli (*40, 41*). The functional relationship of phase resetting, underlying ERP components, to these more general brain dynamic events remains to be explored. Finally, the analysis approach used here, if applied to other types of event-related brain data that are typically averaged, such as optical recordings, neural spike trains, and functional magnetic imaging signals, might reveal additional facts about cortical dynamics (*42*).

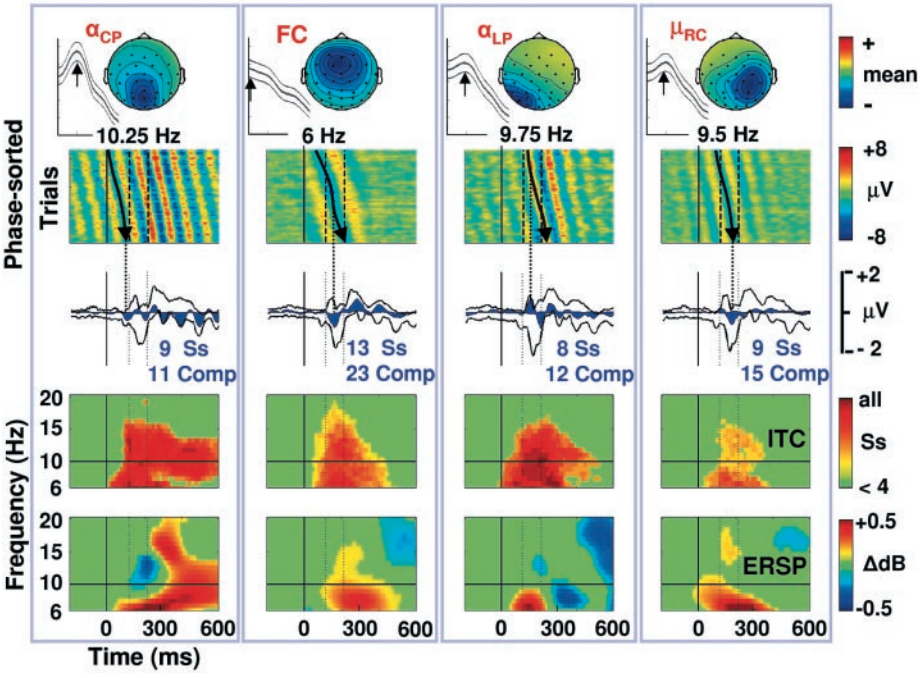

Fig. 4. Characteristics of four of the contributing component clusters (left to right): α_{CP}, central posterior alpha; FC, left frontocentral; α_{LP}, lateral posterior alpha; μ_{RC}, right central mu. Top row: Normalized mean (± SD) log power spectra and cluster-mean scalp maps. Second row: ERP image plots of cluster activity in all single trials, sorted by phase in a three-cycle poststimulus time window at the indicated frequency. Solid vertical lines, stimulus onset; dotted lines, N1 interval. Middle row: Black traces, the envelope (most positive and most negative values at each time point) of the grand-mean ERP for the subjects contributing to each cluster. Blue filled outlines, envelope of the component cluster contribution. Fourth row: For each time and frequency, the number, among all the subjects contributing to the cluster (indicated above), whose cluster component(s) exhibited significant ($P < 0.02$) phase locking (ITC) (*16*) to the stimuli. Green areas, significant ITC in fewer than four subjects. Bottom row: Mean event-related spectral perturbations (ERSPs) (*15*), showing cluster mean differences in log spectral EEG power relative to log power in the 1-s prestimulus EEG baseline.

References and Notes

1. E. Salinas, T. J. Sejnowski, *Nature Rev. Neurosci.* **2**, 539 (2001).
2. B. M. Sayers, H. A. Beagley, W. R. Henshall, *Nature* **247**, 481 (1974).
3. E. Basar, *EEG-Brain Dynamics: Relation Between EEG and Brain Evoked Potentials* (Elsevier, New York, 1980).
4. M. E. Brandt, B. H. Jansen, J. P. Carbonari, *Electroencephalogr. Clin. Neurophysiol.* **80**, 16 (1991).
5. P. Tiesinga, J.-M. Fellous, J. Jose, T. J. Sejnowski, *Neurocomputing* **38**, 587 (2001).
6. S. A. Hillyard, L. Anllo-Vento, *Proc. Natl. Acad. Sci. U.S.A.* **95**, 781 (1998).
7. R. Mangun, in *Induced Rhythms in the Brain*, E. Basar, T. H. Bullock, Eds. (Birkhäuser, Boston, 1992), pp. 219–229.
8. C. Andrew, G. Pfurtscheller, *Neurosci. Lett.* **222**, 103 (1997).
9. W. Lutzenberger, *Int. J. Psychophysiol.* **26**, 273 (1997).
10. Supplementary material is available on *Science* Online at www.sciencemag.org/cgi/content/full/295/5555/690/DC1
11. Five 1.6-cm^2 square outlines indicating possible stimulus locations were permanently displayed 0.8 cm above a central fixation cross. In each 76-s block of trials, one outline was colored green, indicating the target location for that block of trials. Target location was evenly distributed over the five stimulus locations across 30 trial blocks per subject. Stimuli were briefly flashed white circular disks each presented for 117 ms in a randomly selected stimulus location following a randomly selected interstimulus interval of 250 to 1000 ms. Subjects were asked to press a right thumb button press as quickly as possible each time a (target) stimulus appeared in the target location (green box), and to ignore (nontarget) stimuli presented in the other four boxes. EEG data were collected from 29 scalp locations plus two periocular sites, referred to the right mastoid at a rate of 256 Hz/channel with an analog band-pass of 0.01 to 100 Hz. Scalp impedances were kept below 5 kΩ. After rejecting epochs containing out-of-bounds values, data were low-passed below 40 Hz to suppress line noise. See S. Makeig *et al.* [*Philos. Trans. R. Soc. London Ser. B* **354**, 1135 (1999)] and (*12*).
12. J. Townsend, E. Courchesne, *J. Cogn. Neurosci.* **6**, 220 (1994).

13. The expected amplitude of the average of N trials with randomly distributed phase is $1/\sqrt{N}$ of mean single-trial amplitude. On average, the single-subject ERPs were averages of 922 trials, so the expected mean |ERP|/|EEG| amplitude ratio was $1/\sqrt{922} = -29.65$ dB.
14. S. Makeig, *Electroencephalogr. Clin. Neurophysiol.* **86**, 283 (1993).
15. Time/frequency analyses used three-cycle Hanning-windowed sinusoidal wavelets at each frequency moved through the 3-s data epochs (from –1 s before to 2 s after stimulus onset) in 14-ms steps. Event-related spectral perturbation (ERSP) plots showed time/frequency points at which mean log power, across the input epochs, was higher or lower than mean power during the 1-s prestimulus baseline period of the same epochs. The ERSP transform of the averaged ERP data (Fig. 1C) was computed for each scalp channel across the 15 individual-subject ERPs. The ERSP transform of the single-trial epochs (Web. fig. 3B) was computed, for each subject and scalp channel, across a mean of 922 single-trial epochs. Bootstrap $P < 0.02$ significance levels were computed from distributions of ERSP values computed from surrogate data windows drawn at random from the same data epochs.
16. Also referred to as "phase-locking factor." [C. Tallon-Baudry, O. Bertrand, C. Delpuech, J. Pernier, *J. Neurosci.* **16**, 4240 (1996)]. Window lengths, step size, and significance levels were the same as for the power analyses (*15*).
17. These results parallel the demonstration of Sayers *et al.* (*2*) that the averaged auditory ERP in their experiments was produced by a stimulus-induced partial phase resetting of EEG rhythms in single trials.
18. These data used a right mastoid reference. Similar relationships between alpha phase and subsequent ERP morphology have been reported by B. H. Jansen, M. E. Brandt, *Electroencephalogr. Clin. Neurophysiol.* **80**, 241 (1991), and related results in (*19–21*).
19. M. E. Brandt, *Int. J. Psychophysiol.* **26**, 285 (1997).
20. R. Barry, S. Kirkaikul, D. Hodder, *Int. J. Psychophysiol.* **39**, 39 (2000).
21. V. Kolev, J. Yordanova, M. Schurmann, E. Basar, *Int. J. Psychophysiol.* **39**, 159 (2001).
22. S. Makeig, A. J. Bell, T.-P. Jung, T. J. Sejnowski, *Adv. Neural Inf. Process. Syst.* **8**, 145 (1996).
23. T.-P. Jung *et al.*, *Proc. IEEE* **87**, 1107 (2001).
24. A. J. Bell, in *Handbook of Neural Networks*, M. Arbib, Ed., in press.
25. A. J. Bell, T. J. Sejnowski, *Neural Comput.* **7**, 1129 (1995).
26. For each subject, ICA training data consisted of approximately 922 concatenated 52-point, 31-channel data epochs. Initial learning rate was 0.004; training was stopped when learning rate fell below 10^{-6}. Initial block size was 128. Training required less than 30 min per subject on a PC workstation. Source and binary code for the enhanced version (*24*) of the infomax ICA algorithm (*25*) we used are available, together with a MATLAB toolbox for EEG time/frequency analysis and visualization, from www.sccn.ucsd.edu.
27. A relatively large ICA training data set (31 channels by 150,000 time points) was used for maximum stability assuming similar early visual processing in all conditions. Detailed comparisons of different stimulus and attention conditions including target trials will be pursued in future studies.
28. Clustering was based on normalized component activity spectra and scalp maps, and used a modified Mahalanobis distance metric [S. Enghoff, "Moving ICA and time-frequency analysis in event-related EEG studies of selective attention," *INC-9902* (Institute for Neural Computation, La Jolla, CA, 1999)].
29. BESA software (Megis Software, Munich) [M. Scherg, D. v. Cramon, *Electroencephalogr. Clin. Neurophysiol.* **62**, 32 (1985)] was used to fit one or more dipoles to each ICA component scalp map using a four-shell spherical head model.
30. R. Hari, R. Salmelin, J. Makela, S. Salenius, M. Helle, *Int. J. Psychophysiol.* **26**, 51 (1997).
31. G. Pfurtscheller, C. Neuper, G. Krausz, *Clin. Neurophysiol.* **111**, 1873 (2000).
32. S. Makeig, S. Enghoff, T.-P. Jung, T. J. Sejnowski, *IEEE Trans. Rehab. Eng.* **8**, 208 (2000).
33. A. Rougeul-Buser, P. Buser, *Int. J. Psychophysiol.* **26**, 191 (1997).
34. A. Destexhe, T. J. Sejnowski, *Thalamocortical Assemblies* (Oxford Univ. Press, Oxford, 2001).
35. A. K. Engel, P. Fries, W. Singer, *Nature Rev. Neurosci.* **2**, 704 (2001).
36. R. Chapman, J. Stern, J. Engel, M. Cohen, "Tomographic Mapping of Alpha Rhythm Using Simultaneous EEG/fMRI," presented at the 7th Annual Meeting of the Organization for Human Brain Mapping, 10 to 14 June 2001, Brighton, UK (2001).
37. N. Logothetis, J. Pauls, M. Augath, T. Trinath, A. Oeltermann, *Nature* **412**, 150 (2001).
38. J. Klopp, K. Marinkovic, P. Chauvel, V. Nenov, E. Halgren, *Hum. Brain Mapp.* **11**, 286 (2000).
39. T. Mima, T. Oluwatimilehin, T. Hiraoka, M. Hallett, *J. Neurosci.* **21**, 3942 (2001).
40. A. Von Stein, C. Chiang, P. Koenig, *Proc. Natl. Acad. Sci. U.S.A.* **97**, 14748 (2000).
41. M. S. Worden, J. J. Foxe, N. Wang, G. V. Simpson, *J. Neurosci. Online* **20**, RC63 (2000).
42. G. D. Brown, S. Yamada, T. J. Sejnowski, *Trends Neurosci.* **24**, 54 (2001).
43. This research was supported by the Howard Hughes Institute for Medical Research, the NIH [NIMH 2RO1-MH36840 (E.C.) and NINDS 1RO1-NS34155 (J.T.)], the U.S. Office of Naval Research, the U.S. Fulbright Program, and the Swartz Foundation.

12 September 2001; accepted 12 December 2001

RNA Helicase MUT-14–Dependent Gene Silencing Triggered in *C. elegans* by Short Antisense RNAs

Marcel Tijsterman,* René F. Ketting,* Kristy L. Okihara, Titia Sijen, Ronald H. A. Plasterk†

Posttranscriptional gene silencing in *Caenorhabditis elegans* results from exposure to double-stranded RNA (dsRNA), a phenomenon designated as RNA interference (RNAi), or from co-suppression, in which transgenic DNA leads to silencing of both the transgene and the endogenous gene. Here we show that single-stranded RNA oligomers of antisense polarity can also be potent inducers of gene silencing. As is the case for co-suppression, antisense RNAs act independently of the RNAi genes *rde-1* and *rde-4* but require the mutator/RNAi gene *mut-7* and a putative DEAD box RNA helicase, *mut-14*. Our data favor the hypothesis that gene silencing is accomplished by RNA primer extension using the mRNA as template, leading to dsRNA that is subsequently degraded.

RNA interference (RNAi) in animals, co-suppression in plants, and quelling in fungi appear to be manifestations of cellular defense mechanisms against the invasion of foreign nucleic acids such as viruses or transposons. These gene-silencing phenomena share a common reaction intermediate: small RNA molecules [20 to 25 nucleotides (nt) long], designated siRNAs, that are complementary to the silenced locus and target the cognate mRNA for destruction (*1–5*). To study the role of such short RNA molecules in vivo and their dependence on genes required for RNAi (*6*, *7*), we examined whether we could trigger RNAi by injecting either single-stranded RNA (ssRNA) or double-stranded RNA (dsRNA) oligonucleotides into *Caenorhabditis elegans* (*8*).

Exposing *C. elegans* to *pos-1* dsRNA leads to embryonic lethality of the progeny (*6*). Because *pos-1* mRNA is maternally provided, one can administer the RNA oligomers into the immediate vicinity of the mRNA by injecting them into the gonadal syncytium. Injection of dsRNA molecules of 25 base pairs (bp), corresponding to the *pos-1* sequence (either blunt or with a 2-bp 3′ overhang), triggers gene silencing in 5 to 10% of the progeny embryos (Fig. 1). In contrast, injection of identical amounts of long dsRNA (0.8 kb) results in 100% RNAi, which is consistent with RNAi requiring long dsRNA to work efficiently (*5*). For the corresponding 25-oligomer ssRNAs, we found that although the sense oligomer had no effect, the antisense oligomer induced the RNAi phenotype in ~50% of the progeny when one gonad was injected and in 100% when both gonads were injected (Fig. 1A). The sequence context of the trigger did not strongly affect the efficiency of targeting; 25-nt antisense RNAs (asRNAs) complementary to different regions of the *pos-1* mRNA had similar abilities to induce gene silencing (Fig. 1B). The RNA nature of the trigger proved essential: Molecules

Hubrecht Laboratory, Center for Biomedical Genetics, Uppsalalaan 8, 3584 CT, Utrecht, Netherlands.

*These authors contributed equally to this work.
†To whom correspondence should be addressed at Hubrecht Laboratory, Uppsalalaan 8, 3584 CT, Utrecht, Netherlands. E-mail: plasterk@niob.knaw.nl